



 Cite this: *New J. Chem.*, 2022, **46**, 11303

Fast photodegradation of antibiotics and dyes by an anionic surfactant-aided CdS/ZnO nanodispersion

 K. Jia,^a G. Liu,^a D. N. Lang,^a S. F. Chen,^a C. Yang,^a R. L. Wu,^{*a} W. Wang ^{*b} and J. D. Wang^a

The photocatalytic technology has broad applications in energy and environmental science. In this study, we synthesized a type II heterojunction CdS/ZnO (CSZ) nanodispersion by means of one-pot precipitation. Different from previous studies, an anionic surfactant was used to improve the photocatalytic activity of CdS/ZnO. The CdS/ZnO nanodispersion showed very good photocatalytic performance in the degradation of tetracycline (TC) under visible light, with the highest degradation rate of 94.4% when pH = 7, both pH > 7 and pH < 7 were not conducive to TC degradation. Fast and high degradation efficiency was observed for three model compounds, and the degradation efficiency of RhB reached 100%. After 5 cycles, the degradation efficiency remains above 85%. In the photocatalysts, CdS nanoparticles act as photosensitizers, extending the light response of ZnO to the region of visible light, meanwhile, effectively reducing the electron–hole binding rate, which greatly improved the photocatalytic activity. In the end, the photocatalytic enhancement mechanism of TC degradation was discussed.

 Received 9th March 2022,
 Accepted 12th May 2022

DOI: 10.1039/d2nj01187e

rsc.li/njc

Introduction

Overuse of tetracycline (TC) antibiotics in veterinary medicine, aquaculture,¹ and animal husbandry² is a serious problem. Tetracycline has strong antibacterial ability, and its aqueous solution is very stable (pH = 7), which can circulate in our environment through human and animal excrement.³ Under acid and alkaline conditions, TC is easily hydrolyzed to toxic substances which cannot be completely eliminated by wastewater treatment, posing a serious threat to human health and ecological balance.⁴ Therefore, developing effective disposal technologies has been a challenge in both industrial and scientific domains.⁵

Classical treatments of tetracyclines include physical, biological,⁶ and chemical methods.⁷ With the development of semiconductor photocatalysis, the application of the technology is rising rapidly, especially photocatalysis under visible light.^{8,9} Li *et al.*¹⁰ prepared a graphene/g-C₃N₄ composite material using the self-conversion method, and the degradation rate under visible light was about 32 times higher than that of g-C₃N₄. Truong *et al.*¹¹ prepared C₃N₄-WO₃ nanosheets, which had

good photocatalytic efficiency and cycling stability in water. Among the commonly used semiconductor materials (such as TiO₂, ZnO, SnO₂, ZrO₂, and CdS),^{12–15} ZnO shows good photonic stability, low toxicity, and low cost.^{16,17}

Unfortunately, the application of ZnO is limited in the field of photocatalysis for two reasons: (1) ZnO has a high band gap value (3.37 eV) and only responds to ultraviolet light; (2) its electron–hole pairs are very easy to recombine.^{18,19} Coupling ZnO with narrow bandgap semiconductors (such as ZnSe, ZnS and CdS) has become a feasible method to improve its photocatalytic properties.²⁰ The band-gap structure of CdS is similar to that of ZnO, which can be used as the visible sensitizer to ZnO.^{21,22} Zhang *et al.*²³ prepared ZnO/CdS hierarchical heterojunction nanofibers, and bisphenol was completely degraded in 30 min under visible light. Furthermore, catalysts based on ZnO and CdS have received widespread attention due to diverse morphologies and simple preparation methods (*e.g.* precipitation, hydrothermal synthesis, sol–gel process, and electrochemical deposition).^{24–27} In addition, type-II heterostructures of ZnO and CdS can reduce the probability of electron–hole pair recombination, through the space charge separation process.²⁸

In this study, CSZ nanodispersion with high crystallinity was constructed to enhance the optical properties of ZnO. The deposition method and hydrothermal method were used in our synthesis, which are easy to implement. During preparation, SDS was added to prevent the accumulation of ZnO, and increase the adsorption of pollutant molecules on the surface

^a Key Laboratory of Oil & Gas Fine Chemicals Ministry of Education & Xinjiang Uyghur Autonomous Region, School of Chemical Engineering, Xinjiang University, Urumqi, 830046, China. E-mail: wuronglan@163.com

^b Department of Chemistry & Centre for Pharmacy, University of Bergen, Bergen, 5020, Norway. E-mail: wei.wang@uib.no; Fax: +47 55583355; Tel: +47 55583355



of CSZ.²⁹ The band-gap energies of the CSZ photocatalyst are 3.15 eV and 2.55 eV, respectively, which are equivalent to those of CdS and ZnO. The peak intensity of CSZ in the photoluminescence spectrum is lower than that of ZnO, indicating that the electron-hole recombination rate on the surface of CSZ is lower. In addition, we also conducted photocatalytic experiments under irradiation of visible light. Using TC and three dyes as model pollutants, we studied the photocatalytic properties of pure ZnO and CSZ nanodispersions and proposed the photocatalytic mechanism.

Experimental

Materials

Zinc nitrate hexahydrate (>99%), cadmium acetate dihydrate (>99%), sodium hydroxide (>96%), sodium dodecyl sulfate (>99%), thioacetamide (>99%), ethylenediaminetetraacetic acid disodium salt (EDTA-2Na), benzoquinone (BQ), *tert*-butyl alcohol (*t*-BuOH) and tetracycline (TC) were purchased from Tianjin Zhiyuan Chemicals Ltd. Rhodamine B (RhB), methyl orange (MO), and methylene blue (MB) were purchased from Yongsheng Chemicals Ltd. The chemicals were of analytical grade and used as received. Deionized water was used in all experiments.

Synthesis of ZnO

The ZnO photocatalyst is prepared using a simple method of chemical precipitation. First, 50 mL of 0.4 M Zn(NO₃)₂ solution was prepared. Then, sodium lauryl sulphate (0.02 M) and NaOH solution (0.85 M) were added and stirred for 2 h. The product was collected by centrifugation. The precipitate was washed three times with deionized water and ethanol, and dried at 60 °C for 12 h in a vacuum oven. The dry product was calcined at 400 °C for 4 h in a muffle furnace.

Synthesis of CdS/ZnO

The CdS/ZnO photocatalyst was synthesized by a hydrothermal method. ZnO particles (0.25 g) were dispersed in 30 mL of deionized water. Cadmium acetate was added to the dispersion under vigorous stirring at room temperature for 1 h. Subsequently, SDS (0.02 M) was added and stirred for 1 h. Afterward, thioacetamide (TAA) solution was added to the solution with equimolar cadmium acetate. The mixture was stirred for 1 h and then transferred to an autoclave lined with Teflon. The reaction was conducted at 120 °C for 12 h. Finally, the solid products were collected by centrifugation and washed with ethanol and water. The product was dried in a vacuum oven at 60 °C for 12 h. Five CdS/ZnO nanodispersions were synthesized with different molar ratios of CdS/ZnO (0.05, 0.1, 0.2, 0.4 and 0.6), and named CSZ1, CSZ2, CSZ3, CSZ4, and CSZ5, respectively Fig. 1.

Materials characterization

X-Ray powder diffraction (XRD) was carried out using an XRD-6000 diffractometer (Shimadzu) equipped with a Cu κ

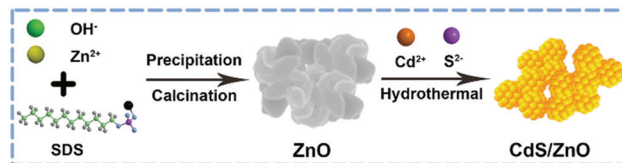


Fig. 1 Synthetic procedure of ZnO and the CdS/ZnO nanodispersion.

radiation source. The range of data collection was from 20° to 80° with an interval of 0.02° per step and a scan speed of 10° min⁻¹. The morphology and crystallinity of the composite were analysed by field emission scanning electron microscopy (FESEM, SU8010, Hitachi, Japan) and high-resolution transmission electron microscopy (HRTEM, JEM-2100, Japan electronics). Using the Brunauer–Emmett–Teller (BET) and Barrett–Joyner–Halenda (BJH) models, surface analysis was conducted. Infrared spectra were recorded using an FTIR VERTEX70 (Bruker, Germany). UV-Visible diffuse reflectance spectroscopy (UV-vis DRS, 750S, PE) was used to measure the absorption intensity of light. An X-Ray photoelectron spectrometer (XPS, ESCALAB 250Xi, American Thermo Fisher Scientific) equipped with an Al radiation source (1486.6 eV) was used to analyse the bonding information. Photoluminescence spectra (PL) were recorded using a fluorescence spectrometer (F-4600, VARIAN, Agilent, USA) with an excitation wavelength of 360 nm. The electron spin resonance (ESR) of spin-captured oxidation radicals was obtained by using a quantum ray Nd:YAG laser system ($\lambda > 420$ nm) with a JES-FA200 ESR (Bruker).

Catalytic activity

The photocatalytic activity was evaluated by the degradation of model pollutants under visible light, which was conducted on a photocatalytic reaction device (XPA-7, Nanjing Xujiang Electromechanical Co., Ltd). A 350W xenon lamp was used as the light source ($\lambda > 420$ nm). The catalyst (20 mg) was dispersed in a 50 mL quartz cell. TC (20 mL, 100 mg L⁻¹) and 30 mL of deionized water were added. The mixture was sonicated to ensure that the catalyst is evenly dispersed in the solution. Then, the quartz tube was put into the reaction device and kept in the dark for 60 minutes to reach the adsorption-desorption equilibrium. After the xenon lamp was switched on, a portion of the supernatant (4 mL) was sampled from the quartz tube every 15 minutes and filtered with a cellulose membrane (0.45 μ m). The absorbance of the samples was determined at 357 nm. The degradation ratio ($1 - C/C_0$) was calculated.

Photoelectrochemistry

Electrochemical measurements were carried out using a Chenhua CHI 660E electrochemical workstation. A three electrode configuration was used with an Ag/AgCl electrode, a Pt electrode, and CdS/ZnO coated FTO glass. For the working electrode, CSZ (7 mg) and Nafion solution (20 μ L, 5%) were dispersed in 1 mL of isopropanol. The mixture was treated in an ultrasonic water bath for 30 min, and a drop (50 μ L) is coated on the FTO glass. This coating procedure was repeated



nine times. Subsequently, the electrodes were vacuum-dried at 60 °C for 12 h. The distance between the light source and the working electrode was 20 cm. The power of the Xe lamp was 300 W with 100 mW cm⁻². For electrochemical impedance spectra (EIS), the voltage amplitude of 5 mV AC with a frequency range of 10² to 10⁵ Hz was used. The frequency of the Mott-Schottky curve is 1000 Hz.

Results and discussion

Structural, morphological, chemical, and optical properties

The crystal structures of the catalysts were analysed by XRD (Fig. 2). Pure ZnO shows diffractive patterns at $2\theta = 31.76^\circ$, 34.42° , 36.25° , 47.54° , 56.61° , 62.86° , 66.38° , 67.96° , 69.10° , 72.56° , and 76.95° corresponding to the standard diffraction of the (100), (002), (101), (102), (110), (103), (200), (112), (201), (004) and (202) planes (JCPDS File NO. 36-1451),^{30,31} respectively. These crystal planes are consistent with the hexagonal wurtzite structure. The sharp diffraction peaks indicate high crystallinity.³² Pure CdS shows diffraction peaks at $2\theta = 26.51^\circ$, 43.98° , and 52.10° , corresponding to the (111), (220), and (311) crystal planes of face-centered cubic CdS (JCPDS File NO. 42-1411).³³ The characteristic peaks of CdS and ZnO can be identified in the XRD spectra of CSZ. With an increase in the CdS composition, the peak intensity of the CdS phase increases significantly. No impurity peaks of ZnS or Zn(OH)₂ were found, meaning that the complexation of CdS does not affect the phase structure of ZnO.

Fig. 3a–c show the FESEM images of ZnO, CdS, and CSZ4, respectively. ZnO nanoparticles showed irregular shapes with smooth surfaces. For pure CdS, nanoplatelets of CdS aggregated to a spherical shape with sizes of 1.5–2 μm. For CSZ4, small nanoparticles with a size of 40–60 nm were observed with protrusions on the surface. The average size of CSZ4 is about 54 nm (Fig. 3f). The size of CSZ is smaller than the size of ZnO and CdS nanoparticles. The HRTEM image (Fig. 3d) further shows the raspberry-like nanosphere morphology of CSZ4 with

a uniform size. The lattice fringe of CSZ4 (Fig. 3e) exhibited both ZnO and CdS crystal faces. The lattice fringes of 0.191 nm, 0.260 nm, and 0.245 nm correspond to the (102), (002), and (101) facets of ZnO, respectively. The lattice fringes of 0.335 nm, 0.175 nm, and 0.205 nm correspond to the (111), (311), and (220) crystal planes of CdS, respectively. These results are consistent with XRD analysis. Elemental mapping (Fig. 3g–k) was used to study the dispersion of each element in CSZ4. Zn, Cd, S, and O elements are evenly distributed. Therefore, we can conclude that CdS and ZnO are fully combined, which is conducive to the separation and transfer of photogenerated carriers.

The specific surface area and pore size distribution of the photocatalysts were studied by nitrogen adsorption–desorption isotherms (Fig. 4). Fig. 4a shows the adsorption and desorption isotherms of ZnO and CSZ4. Both ZnO and CSZ4 exhibit type IV isotherms with obvious H3 hysteresis loops, which indicate that the samples have mesoporous structures.^{34,35} Active sites play an important role in photocatalysis.³⁶ Photocatalysts with large specific surface areas are generally considered to have more active sites. The specific surface areas of ZnO and CSZ4 are 4.313 and 16.365 m² g⁻¹, respectively, confirming that the CSZ4 composite has a larger specific surface area than ZnO after adding CdS. This improvement may be due to the microporous structure which increases the surface roughness and reduces the crystal size,³⁷ which also corresponds to the reduction of the size for CSZ4. The large specific surface area provides more active sites on the CSZ4 surface,³⁸ which is conducive to the adsorption and reaction of pollutant molecules on the surface. The pore size distribution of ZnO and CSZ4 is presented in Fig. 4b and c, respectively. According to the BJH model, the pore volumes of ZnO and CSZ4 were 0.018 and 0.066 cc g⁻¹, respectively, and the average pore sizes were 3.055 and 3.066 nm, respectively.

The bonding energy of CSZ4 was studied by XPS. Zn, Cd, S, and O elements are observed in the survey spectrum (Fig. 5a). Fig. 5b shows the curve fitting spectrum of Zn 2p. There are two significant peaks at 1021.52 eV and 1044.55 eV, which are attributed to 2p_{3/2} and 2p_{1/2} of Zn, respectively, and correspond to Zn²⁺ in the ZnO crystal.³⁸ In the O 1s spectrum (Fig. 5c), 529.58 eV is the lattice oxygen in ZnO, and 531.23 eV is the oxygen vacancy. In the Cd 3d spectrum (Fig. 5d), the peaks of 404.66 eV and 411.45 eV are from Cd 3d_{5/2} and Cd 3d_{3/2}, respectively.³⁹ The S 2p spectrum in Fig. 5e shows two peaks at 161.07 eV and 162.28 eV, which are attributed to S 2p_{3/2} and S 2p_{1/2}, respectively.⁴⁰

FTIR was used to study the surface groups and chemical bonds of the prepared photocatalyst (Fig. 5f). The sharp peaks at 477 cm⁻¹ and 612 cm⁻¹ are characteristic peaks of the Zn–O bond and the Cd–S bond, respectively.^{32,41} The absorption band at 1556 cm⁻¹ is assigned to the O–H bending vibrations of H₂O, and that at 3430 cm⁻¹ corresponds to the tensile vibration mode.⁴² In addition, the vibration peaks at 2929 and 2851 cm⁻¹ are the stretching vibrations of –CH₂.⁴³ The stretching vibration of S=O (1112 cm⁻¹) indicates the presence of SDS on the surface of the catalyst.⁴⁴ The blue shift of the

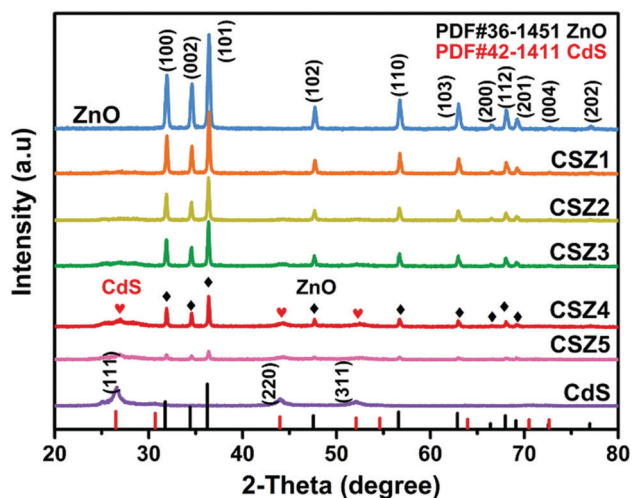


Fig. 2 XRD patterns of ZnO, CdS, and CSZ catalysts.



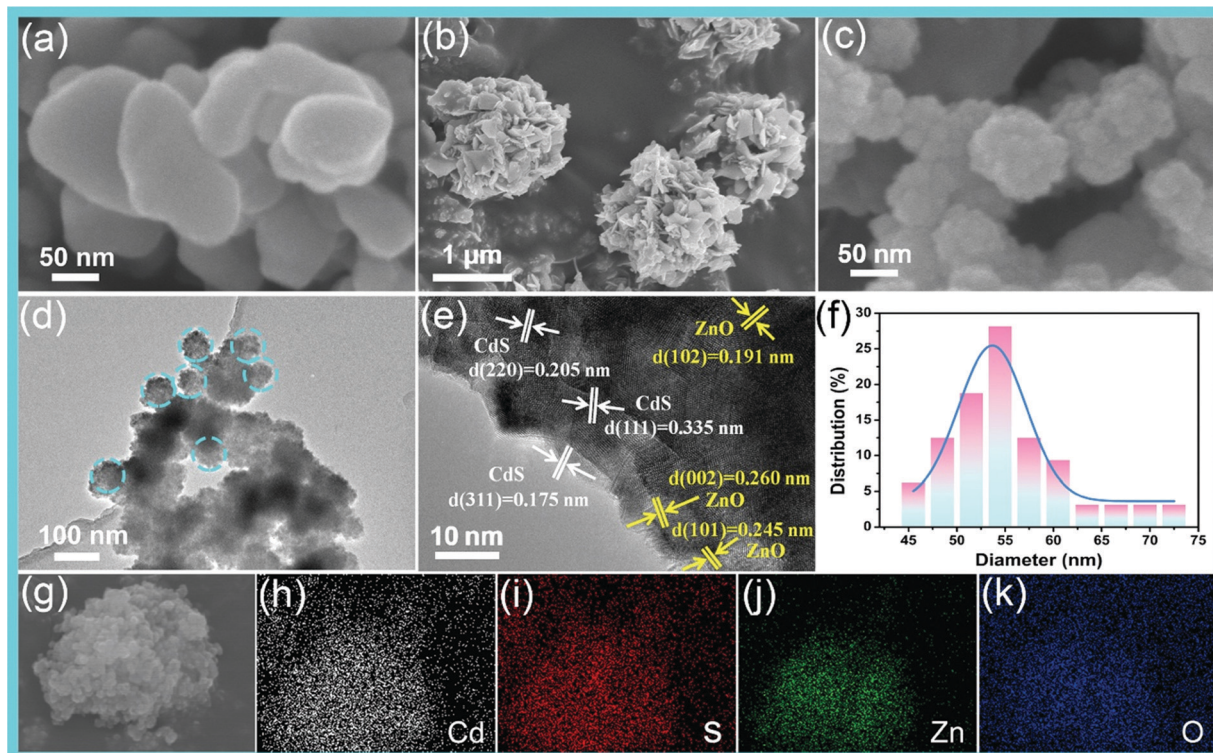


Fig. 3 FESEM images of (a) ZnO, (b) CdS and (c) CSZ4; (d and e) HRTEM images of CSZ4; (f) size distribution of CSZ4; and (g–k) elemental mapping of CSZ4.

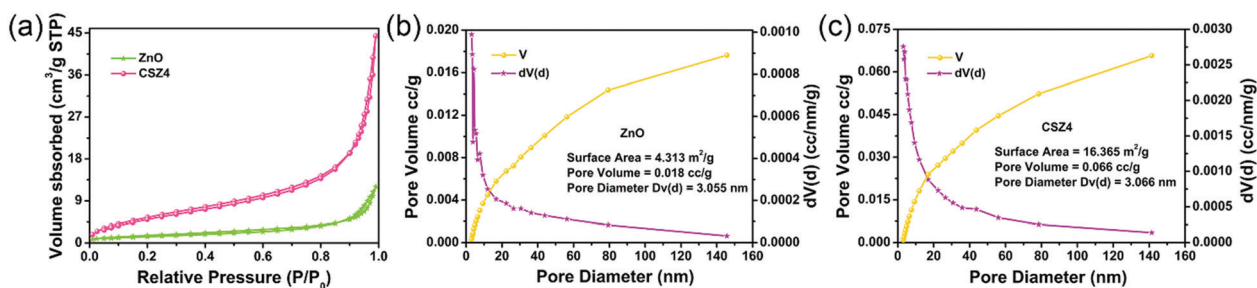


Fig. 4 (a) Nitrogen adsorption–desorption isotherms of ZnO and CSZ4; pore size distribution of (b) ZnO and (c) CSZ4.

1621 cm⁻¹ peak was found in CSZ, indicating that CdS compounds with ZnO form a composite.²⁸

UV-vis DRS was used to analyse the optical properties of the materials and calculate the energy band value of CSZ. The absorption band edge of pure ZnO appears at 390 nm (Fig. 6a), which is due to the absorption of the intrinsic bandgap of ZnO.⁴⁵ The characteristic band edge of CdS is at 550 nm. The absorption band edge of CSZ composites is at around 500 nm, indicating that the addition of CdS moved the absorption of ZnO from the ultraviolet region to the visible region. The results of UV-vis DRS prove that the CSZ composite has a visible light response, which is consistent with the photocatalytic experiment results. Fig. 6b shows the Tauc relationship,⁴⁶ and the straight line is extrapolated and yields the energy band value, where the band gap energies (E_g) are 3.27 eV and 2.33 eV for ZnO and CdS, respectively. In addition, the E_g values of CSZ4

are 3.15 eV and 2.55 eV (Fig. 6c), indicating that it can effectively absorb visible light.

Transient photoluminescence spectra (Fig. 6d) provide information on the recombination rate of photo-generated electron–hole pairs, and the lower the luminescence intensity means the faster separation of electron–hole pairs, thereby improving the photocatalytic activity.⁴⁷ When the excitation wavelength is 360 nm, the emission peaks of ZnO and CSZ appear at 564 nm. The ZnO peak is the highest, indicating that the photoinduced electron–hole pair recombination rate of ZnO is the highest. The addition of CdS reduced the peak value and the peak value decreased with the increase of the CdS content, suggesting that the combination of CdS and ZnO promoted the separation of photogenerated electron–hole pairs, thus effectively improving the photocatalytic activity.⁴⁸



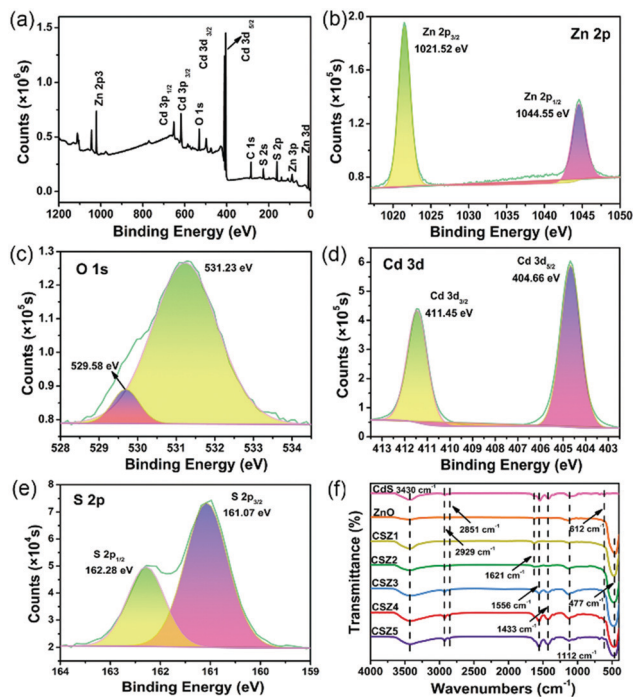


Fig. 5 XPS spectra of CSZ4: (a) survey spectrum, (b) Zn 2p, (c) O 1s, (d) Cd 3d, and (e) S 2p. (f) FTIR spectra of ZnO, CdS and CSZ catalysts with different compositions.

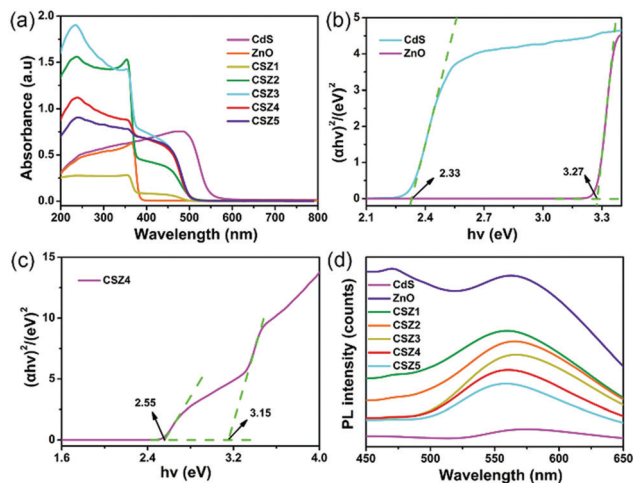


Fig. 6 (a) Diffused reflectance spectra; Tauc plots for the determination of the bandgap energies of (b) ZnO, CdS and (c) CSZ4 catalysts; (d) transient PL spectra of ZnO, CdS, and CSZ catalysts.

Electrochemical properties

The charge transfer characteristics in the catalyst were evaluated by photocurrent intensity and electrochemical impedance spectroscopy. Transient photocurrent is formed by the directional movement of electrons generated when the catalyst is exposed to light.⁴⁹ Fig. 7a shows the photocurrent intensity of ZnO, CdS, and all CSZ under several cycles of light irradiation. All catalysts showed a photocurrent response. The highest photocurrent intensity was observed for CSZ4, which proves

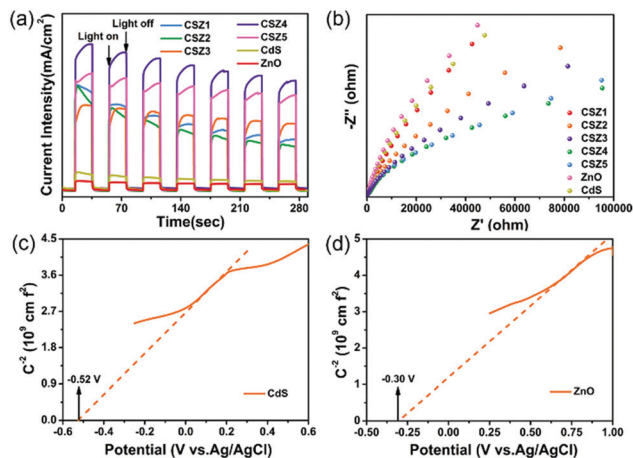


Fig. 7 (a) Transient photocurrent response and (b) EIS Nyquist plot of ZnO, CdS and CSZ catalysts; Mott-Schottky curve of (c) CdS and (d) ZnO (frequency is 1000 Hz).

that more photoelectron-hole pairs are generated in CSZ4. When the light is turned off, the intensity drops to zero instantly, indicating the rapid recombination of carriers. The above results show that the right amount of CdS (0.04) in the composite can accelerate the transfer of carriers, and the separation efficiency of photogenerated electron-hole pairs is the highest. In the course of 7 cycles, the current density of CSZ4 decreased due to the photo-corrosion effect of CdS that consumes electrons on the catalyst surface, resulting in reduced catalytic activity.⁵⁰ This also corresponds to the decline of the catalytic efficiency in the cycling stability experiments. Generally, the larger the photocurrent in the photonic crystal, the smaller the arc radius in the AC impedance in the Nyquist diagram, and the better the separation of photogenerated electron-hole pairs.⁵¹ Electrochemical impedance results (Fig. 7b) show that the arc radius of CSZ4 is smaller than that of ZnO, indicating that the electron has the lowest resistance during transport, which facilitates carrier migration.

The conductivity types and Fermi energy levels (E_f) of ZnO and CdS were analysed by the Mott-Schottky method.^{52,53} The intersection point of a Mott-Schottky diagram of the material at a frequency of 1000 Hz is E_f .⁵⁴ In Fig. 7c and d, the positive slopes of the linear region indicate the n-type characteristics of ZnO and CdS, which can form type II heterojunction.⁵⁵ For ZnO and CdS, the permitted E_f are -0.30 V and -0.52 V (vs. NHE), respectively. Under visible light irradiation, holes and electrons are generated in the valence band (VB) and conduction band (CB), respectively. The active species produced by the reaction between carriers and pollutants can decompose TC effectively. The CB and VB of CdS and ZnO can be calculated by Mulliken electronegativity theory:⁵⁶⁻⁵⁸

$$E_{VB} = \chi - E_C + 0.5E_g \quad (1)$$

$$E_{CB} = E_{VB} - E_g \quad (2)$$

where E_{VB} and E_{CB} are the VB and CB potential energies of the photocatalyst, respectively. The standard hydrogen electrode



potential E_C is about 4.5 eV. The absolute electronegativity χ of the semiconductor photocatalyst is 5.79 and 5.05 eV for ZnO and CdS, respectively.^{56–58} Therefore, the E_{VB} and E_{CB} values of 2.93 and -0.34 eV are obtained for the ZnO photocatalyst, respectively, while those of the CdS photocatalyst are 1.72 and -0.61 eV, respectively. These values are consistent with those in the previous study.⁵⁹

Photodegradation of TC

The degradation experiment is to evaluate the catalytic activity of the catalysts under visible light (350 W, $\lambda > 420$ nm). Fig. 8a shows the results of the adsorption of TC and the degradation of TC by visible light. Adsorption of TC was carried out in darkness and the adsorption–desorption equilibrium was reached in about 1 h. The adsorbed percentages of TC by ZnO, CdS and CSZ(1–5) catalysts are 31.9%, 17.1%, 40.5%, 45.1%, 45.6%, 46.4% and 48.9%, respectively. The amounts of adsorbed TC by CSZ composites are higher than that of ZnO, which is consistent with BET results, and the adsorption of CSZ increases gradually with the increase of the CdS composition, indicating that the addition of CdS is conducive to the adsorption of TC on CSZ. The adsorption of pollutants on catalysts before light irradiation can enhance photocatalytic degradation has been suggested by previous studies.^{60,61} Pre-adsorption provides enough substances for degradation in the next step.

During degradation, the TC concentration remained stable in the control group without adding the catalyst.⁶² In Fig. 8a, the C/C_0 values of TC reduced after 120 minutes of visible light irradiation. The concentration reduced to 41.8% and 65.3% for ZnO and CdS, respectively. The reason why ZnO can degrade TC in visible light may be due to the absorption of visible light by TC adsorbed on ZnO, resulting in self-sensitization.⁶³ The addition of SDS increases the adsorption of TC.⁶⁴ All CSZ catalysts showed better performance than ZnO. Among them,

the CSZ4 composite showed a maximum efficiency of 94.4%. The type II photocatalyst heterojunction formed by the addition of CdS led to the separation of electron–hole pairs in space and enhanced the absorption of visible light of the catalyst, thus greatly improving the activity of ZnO.⁵⁵ The rate constants are presented in Fig. 8b, and the linear fitting was consistent with the first-order kinetics. Among them, the rate constant for CSZ4 showed the highest value of 0.0241 min^{-1} . This value is 5.15 times higher than that for pure ZnO nanoparticles. Fig. 8c shows the UV-visible spectra of TC solution irradiated with visible light at different time intervals in the presence of CSZ. In the presence of CSZ4, the maximum absorption peak at 357 nm disappeared after 90 min.

Photodegradation of RhB, MO, and MB

Because CSZ4 has the best photocatalytic activity, the degradation of RhB, MO, and MB was conducted. Fig. 8d shows the photocatalytic activity of CSZ4 in 120 min. The solution became colourless. The degradation efficiency of RhB, MO, and MB reached 99.6%, 95.9% and 92.2%, respectively.

Effect of pH

The degradation of TC by CSZ4 was studied at different pH values (pH = 3, 5, 7, 9, 11), as shown in Fig. 9. Both acidic and alkaline conditions exerted adverse effects on the degradation of TC by CSZ4. The degradation rate followed the order of neutral > alkaline > acidic. Previous studies also showed that the degradation of pollutants was faster under alkaline conditions than under acidic conditions.^{65,66} The slowest degradation of TC under acidic conditions (pH = 3) may be due to the agglomeration of CSZ4 at low pH, which reduces the adsorption of TC on the surface of the photocatalysts. TC decomposes under alkaline conditions.⁶⁷ Therefore, the change in the TC concentration over time at different pH values without CSZ4 was investigated (Fig. 9c). As expected, TC self-decomposed under alkaline conditions and accelerated when exposed to light. Colour changes in the degradation process are shown in Fig. 9d. When no catalyst is added and pH is > 7, the colour of the TC solution gradually turns pink and purple with the increase of the irradiation time due to self-decomposition. The colour of the TC solution after the self-decomposition clearly shows that the end-product of self-decomposition is different from the colourless products after the photodegradation. When $\text{pH} \leq 7$, no colour change was observed. In the presence of CSZ4 and in the dark environment, TC solution showed a colour change under both acid and alkaline conditions. It is more obvious when $\text{pH} > 7$, indicating TC self-decomposition. With the increase in irradiation time, the solutions of all pHs gradually became colourless under the catalytic action of CSZ4.

UV-Vis spectra also confirmed the degradation performance of CSZ4 at different pH values (Fig. 10). At $\text{pH} > 7$, the maximum absorption wavelength shifts to 367 nm (Fig. 10c and d), and a new peak appears at 532 nm, which corresponds to the colour of the self-decomposition product. Upon irradiation, the peak at 367 nm gradually decreased, while the peak at

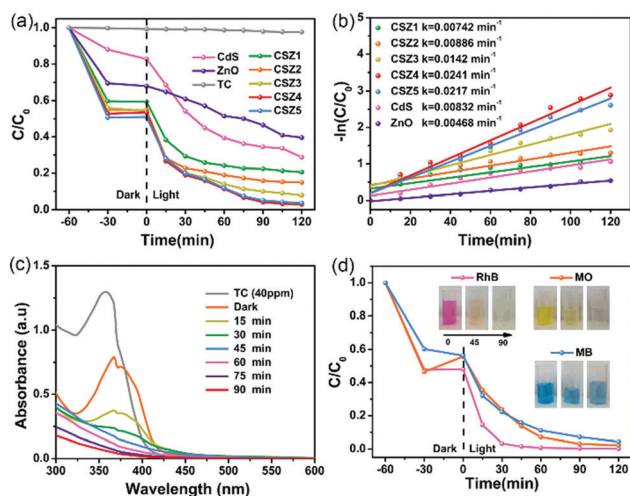


Fig. 8 (a) Photodegradation of TC by the catalysis of ZnO, CdS and CSZ nanodispersions; (b) degradation kinetics analyzed by a pseudo first-order reaction; (c) UV-visible spectra of TC solution irradiated with visible light at different time intervals in the presence of CSZ4; (d) photodegradation of RhB, MO and MB by CSZ4.



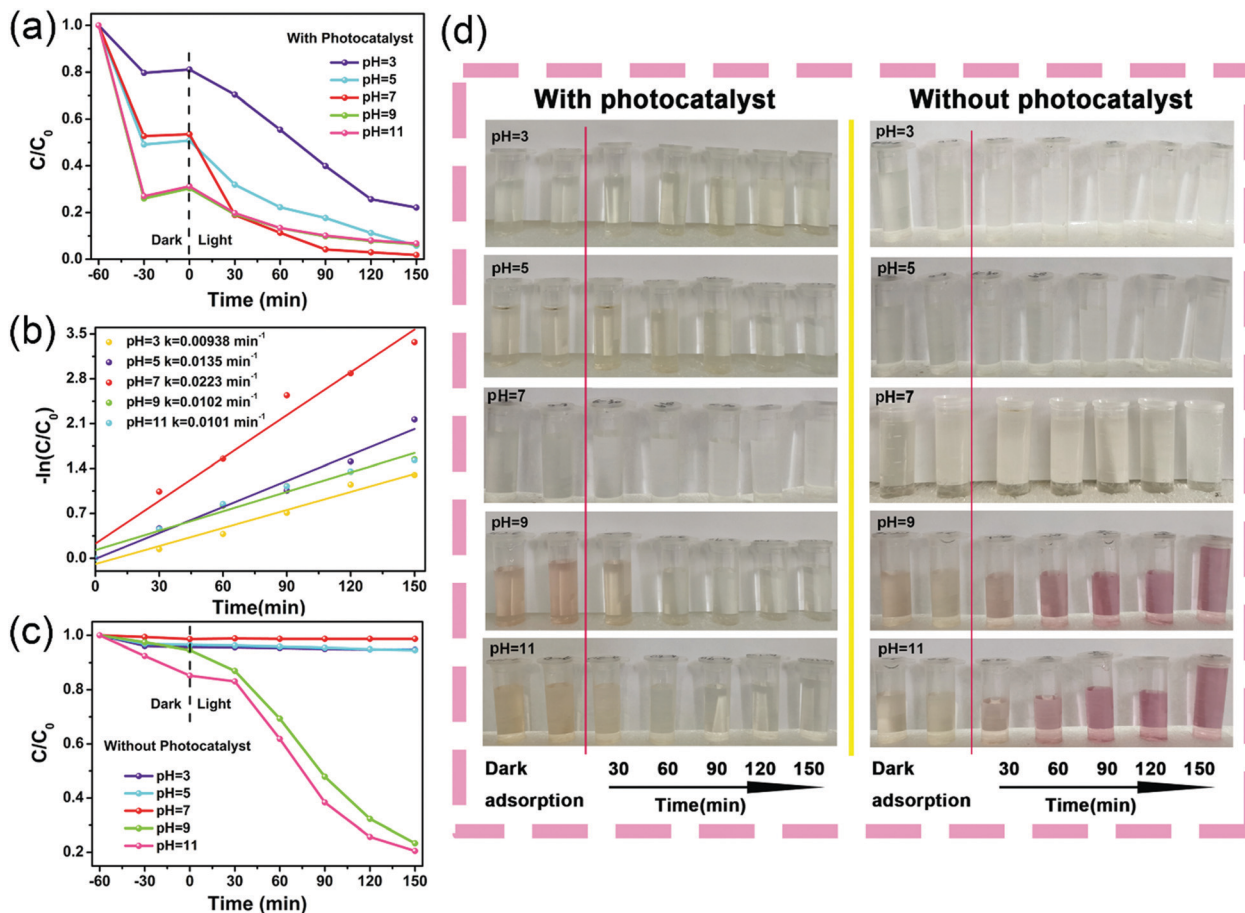


Fig. 9 Degradation curves of TC at different pH values (a) with CSZ4, (c) without CSZ4; (b) the degradation kinetics curve with CSZ4; (d) color change of TC solution with time at different pH values.

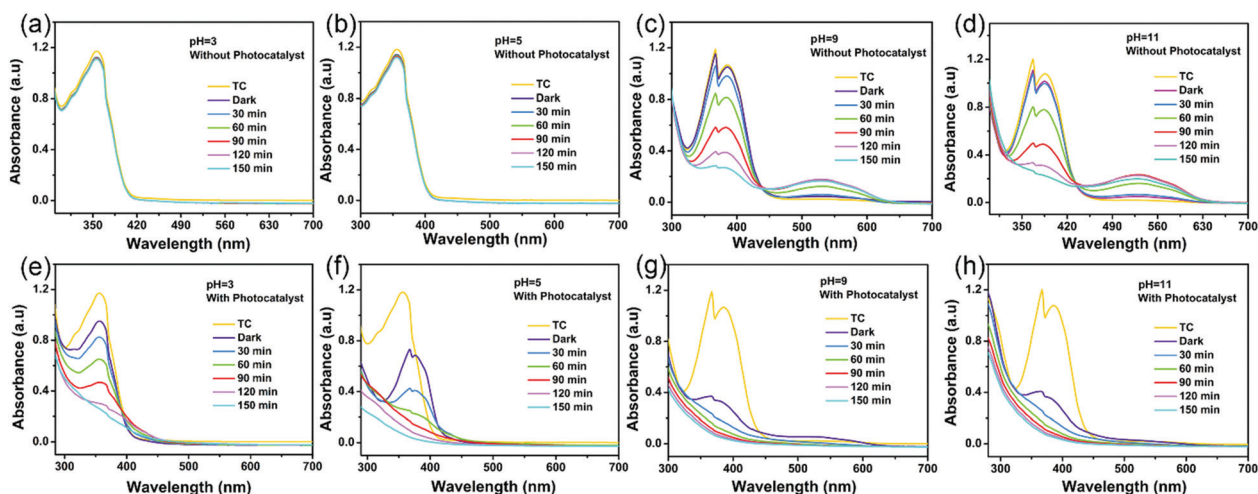


Fig. 10 UV-Vis spectra of the catalysts degraded TC at pH = 3, 5, 9, and 11 (a–d) without CSZ4 and (e–h) with CSZ4.

532 nm increased. Under alkaline conditions, the hydroxyl group on C_6 forms oxygen anions, which undergoes an intramolecular nucleophilic attack on C_{11} . After electron transfer, the C ring is broken to form an isomer with a lactone structure.⁶⁷

In the presence of CSZ4, no peak at 532 nm is observed (Fig. 10g and h), corresponding to a change in the color of TC solution from pink to transparent. At $\text{pH} \leq 7$, no changes in the spectra were observed without a photocatalyst (Fig. 10a and b); with the



photocatalyst, the products of photodegradation were transparent (Fig. 10e and f).

Active species analysis

Active species generated during the photocatalytic procedure were analysed by trapping experiments and ESR. In the trapping experiments, benzoquinone was applied as an $\cdot\text{O}_2^-$ scavenger, *t*-BuOH as a scavenger for $\cdot\text{OH}$, and EDTA-2Na as a scavenger for h^+ , respectively (Fig. 11a).⁶⁸ Obviously, the inhibition degree of the trapping agent from large to small was benzoquinone > EDTA-2Na > *t*-BuOH, indicating that $\cdot\text{O}_2^-$ is the main active species during the degradation process, h^+ is the secondary, while $\cdot\text{OH}$ has little effect during the process. ESR was used to identify the active free radicals (Fig. 11b–d). After irradiation, six peaks in the ESR spectra were determined, which were characteristic peaks of $\cdot\text{O}_2^-$ (Fig. 11b).⁶⁹ The characteristic peaks are very strong, indicating that a large amount of $\cdot\text{O}_2^-$ is produced under irradiation. Fig. 11c shows the characteristic peaks of h^+ . The difference is that similar signals were detected under dark and light conditions, and their intensities decreased slightly with the increase of irradiation time, indicating the presence of h^+ in the photocatalytic reaction system generation and enhancement.⁷⁰ Fig. 11d shows the characteristic peak of $\cdot\text{OH}$.⁷¹ Compared with the steady signal in darkness, only four weak characteristic peaks of $\cdot\text{OH}$ are displayed after illumination. The signals are not sharp and smooth indicating that the amount of $\cdot\text{OH}$ generated is small. In conclusion, the intensities of the characteristic peaks of $\cdot\text{O}_2^-$ and h^+ are higher than that of $\cdot\text{OH}$, meaning that $\cdot\text{O}_2^-$ and h^+ radicals participate in photocatalytic reactions and play a crucial role in TC degradation. The results are consistent with the results of the active species capture experiment.

Photodegradation mechanism

Based on the UV-vis DRS results, Mott–Schottky curve and Mulliken electronegativity theory, the band structure of CSZ, the redox potential of the catalyst surface and the photogenerated electron–hole pair transfer mechanism can be determined,

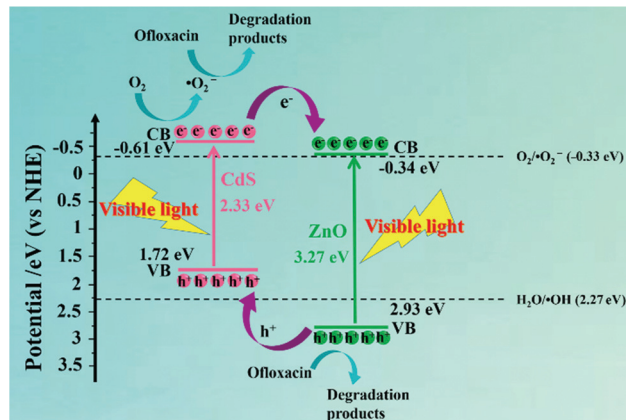


Fig. 12 The energy position of the CSZ composite and the mechanism of photogenerated electron–hole pair transfer.

as shown in Fig. 12. CdS acting as a charge carrier can provide high-speed charge channels in CSZ. Under the irradiation of visible light, the photogenerated electrons generated on the CdS(CB) will transfer to the ZnO(CB). Since the E_{CB} of CdS (-0.61 eV vs. NHE) is more negative than that of ZnO (-0.34 eV vs. NHE), the generation of $\cdot\text{O}_2^-$ tends to occur at the CdS(CB). Then the photogenerated electrons react with oxygen in water to form $\cdot\text{O}_2^-$ ($\text{O}_2/\cdot\text{O}_2^- = -0.33$ eV vs. NHE), which can effectively oxidize organic pollutants.⁷² At the same time, the photogenerated holes from the ZnO(VB) will reversely move to the CdS(VB), and then water is oxidized at the ZnO(VB) to form a $\cdot\text{OH}$ radical ($\text{H}_2\text{O}/\cdot\text{OH} = 2.27$ eV vs. NHE). The h^+ in ZnO(VB) can also oxidize organic pollutants due to the inherent capacity of the photogenerated holes. The construction of a type II heterojunction provides CdS/ZnO with stronger redox ability. Moreover, the synergistic effect of ZnO and CdS promotes the continuous separation of electron–hole pairs.⁷³ Therefore, the CSZ nanocomposite has higher electron–hole separation efficiency than pure ZnO, thus improving its photocatalytic performance. The photocatalytic process is summarized by the reaction equations (eqn (3)–(6)):⁷⁴

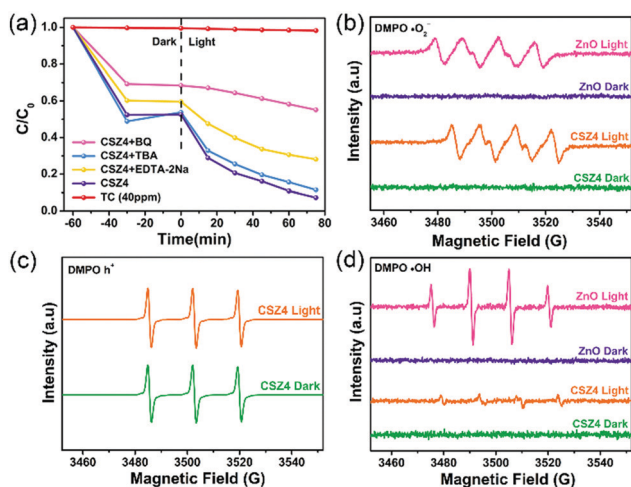
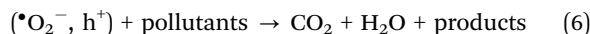
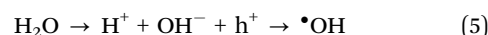


Fig. 11 (a) Radical trapping results of CSZ4; ESR spectra of DMPO spin trapping (b) $\cdot\text{O}_2^-$, (c) h^+ , and (d) $\cdot\text{OH}$.

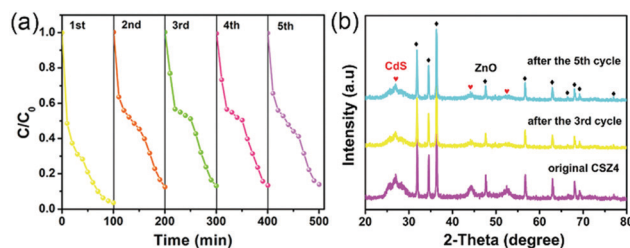


Fig. 13 CSZ4: (a) cycle degradation pattern; (b) XRD pattern before and after the cycle.



Table 1 List of the applications of different catalysts for the photocatalytic degradation of TC and dyes

| Photocatalyst | Pollutant | Dosage (mg) | Pollutant concentration (mg L ⁻¹) | Light source | Rate constant (min ⁻¹) | Ref. |
|--|-----------|-------------|---|--|------------------------------------|-----------|
| Ag/Bi ₃ O ₄ Cl | TC | 50 | 10 | 250 W Xenon lamp ($\lambda > 420$ nm) | 0.0232 | 75 |
| TiO ₂ /TiF ₂ | TC | 40 | 10 | 500 W Xenon lamp ($\lambda > 420$ nm) | 0.0184 | 76 |
| Ag ₂ O/AgBr-CeO ₂ | TC | 25 | 10 | 500 W Xenon lamp ($\lambda > 420$ nm) | 0.0401 | 77 |
| BiOI/g-C ₃ N ₄ | TC | 10 | 20 | 250 W Xenon lamp ($\lambda > 420$ nm) | 0.0246 | 78 |
| Ag/g-C ₃ N ₄ /LaFeO ₃ | TC | 20 | 10 | 300 W Xenon lamp ($\lambda > 420$ nm) | 0.0167 | 79 |
| CdS/ZnO | TC | 20 | 40 | 350 W Xenon lamp ($\lambda > 420$ nm) | 0.0241 | This work |
| CdS/ZnO | MB | 50 | 10 | Visible light | 0.0242 | 80 |
| rGO/ZnO/CdS | MB | 20 | 3.2 | 100 W halogen lamp | 0.0280 | 81 |
| CdS/ZnO | RhB | 200 | 2000 | 3000 W Xenon lamp | 0.0106 | 82 |
| CdS/ZnO | RhB | 15 | 20 | 200 W Sun lamp | 0.0132 | 83 |
| CdS/ZnO | RhB | 20 | 10 | 350 W Xenon lamp ($\lambda > 420$ nm) | 0.0441 | This work |
| | MO | | | | 0.0284 | |
| | MB | | | | 0.0204 | |

Light stability and reusability evaluation

The cyclic degradation was used to evaluate the practical value of CSZ photocatalysts. Five consecutive cycles of TC degradation were performed (Fig. 13a). The degradation efficiency of TC remained above 85% after 5 cycles. In addition, the structural stability of the CSZ photocatalysts was confirmed by XRD (Fig. 13b). After 5 cycles, the characteristic peaks of CdS decrease due to photo-corrosion. The XRD patterns of the third cycle and the fifth cycle are not vastly different, indicating the slow decline of catalytic performance after the second cycle.

In this work, a CdS/ZnO photocatalyst was used for the degradation of TC and dyes. Compared with those obtained from other photocatalysts, the efficiencies of the prepared composite catalysts are summarized in Table 1. Different catalysts were compared in terms of catalyst dosage, pollutants and concentrations, light source, and reaction kinetic constants. The initial concentration of TC degradation by the prepared catalyst is the highest, 40 ppm, and the degradation rate is in the middle. In our study, the rate constants of degradation were also high, indicating that the catalysts showed excellent photocatalytic properties.

Conclusions

In summary, type II heterojunction CdS/ZnO nanocomposites with excellent visible light-trapping ability and high electron-hole separation efficiency were successfully prepared. The content of CdS in CdS/ZnO was adjusted by changing the amount of cadmium acetate during preparation. The addition of CdS significantly increased the specific surface area of the CSZ photocatalyst (16.365 m² g⁻¹), resulting in a large amount of adsorption and photodegradation of TC and dye on the active site. CSZ4 showed the lowest electron-hole recombination rate, and its photocatalytic activity is higher than that of pure CdS or the ZnO photocatalyst. In addition, CSZ4 showed good photocatalytic activity for a high concentration of TC, as well as RhB, MO, and MB under visible light. During the photodegradation, •O₂⁻ played a significant role in studying the reaction mechanism of CdS/ZnO. After 5 cycles, the resultant catalysts still show high catalytic activity, indicating good

potential in the detoxification of sewage containing dyes and tetracyclines.

Conflicts of interest

There are no conflicts to declare.

Acknowledgements

This work was supported by the National Natural Science Foundation of China (21868036 and 32061133005) and the Tianshan Youth Program (2020Q011). We acknowledge the Key Laboratory test Platform of the Ministry of Oil and Gas Fine Chemicals and the facilities and staff at the Scientific Compass research Service.

References

- Q. F. Zhong, Q. T. Lin, R. L. Huang, H. Y. Fu, X. F. Zhang, H. Y. Luo and R. B. Xiao, Oxidative degradation of tetracycline using persulfate activated by N and Cu codoped biochar, *Chem. Eng. J.*, 2020, **380**, 122608–122617.
- I. Michael, L. Rizzo, C. S. McArdell, C. M. Manaia, C. Merlin, T. Schwartz, C. Dagot and D. Fatta-Kassinos, Urban wastewater treatment plants as hotspots for the release of antibiotics in the environment: a review, *Water Res.*, 2013, **47**, 957–995.
- D. M. Ma, W. Y. Liu, Q. Chen, Z. Jin, Y. Zhang, J. Huang, H. Zhang, F. M. Peng and T. Luo, Titanium-oxo-clusters precursors for preparation of In₂S₃/TiO₂ heterostructure and its photocatalytic degradation of tetracycline in water, *J. Solid State Chem.*, 2021, **293**, 121791–121800.
- J. Zhang, L. N. Qu, Y. H. Wu, Y. X. Ma, Z. L. Chai and X. J. Wang, Fabrication of visible-light-driven Bi₂O₃-Bi₃TaO₇ nanocomposite for tetracycline degradation with enhanced photocatalytic efficiency, *J. Solid State Chem.*, 2019, **278**, 120894–120901.
- X. Yuan, S. L. Qu, X. Y. Huang, X. A. Xue, C. L. Yuan, S. W. Wang, L. Wei and P. Cai, Design of core-shelled



- g-C₃N₄@ZIF-8 photocatalyst with enhanced tetracycline adsorption for boosting photocatalytic degradation, *Chem. Eng. J.*, 2021, **416**, 129148–129160.
- 6 M. Işık and D. T. Sponza, Anaerobic/aerobic treatment of a simulated textile wastewater, *Sep. Purif. Technol.*, 2008, **60**, 64–72.
 - 7 W. L. Shi, K. K. Shu, H. R. Sun, H. J. Ren, M. Y. Li, F. Y. Chen and F. Guo, Dual enhancement of capturing photogenerated electrons by loading CoP nanoparticles on N-deficient graphitic carbon nitride for efficient photocatalytic degradation of tetracycline under visible light, *Sep. Purif. Technol.*, 2020, **246**, 116930–116938.
 - 8 X. Xu, K. Jia, S. F. Chen, D. N. Lang, C. Yang, L. Wang, R. L. Wu, W. Wang and J. D. Wang, Ultra-fast degradation of phenolics and dyes by Cu₂O/Cu catalysts: Synthesis and degradation kinetics, *J. Environ. Chem. Eng.*, 2021, **9**, 105505–105513.
 - 9 X. B. Li, J. Y. Liu, J. T. Huang, C. Z. He, Z. J. Feng, Z. Chen, L. Y. Wan and F. Deng, All organic S-scheme heterojunction PDI-Ala/S-C₃N₄ photocatalyst with enhanced photocatalytic performance, *Acta Phys.-Chim. Sin.*, 2021, **37**, 2010030.
 - 10 F. Li, M. Tang, T. Li, L. L. Zhang and C. Hu, Two-dimensional graphene/g-C₃N₄ in-plane hybrid heterostructure for enhanced photocatalytic activity with surface-adsorbed pollutants assistant, *Appl. Catal., B*, 2020, **268**, 118397–118433.
 - 11 H. B. Truong, B. T. Huy, S. K. Ray, Y. Lee, J. Cho and J. Hur, H₂O₂-assisted photocatalysis for removal of natural organic matter using nanosheet C₃N₄-WO₃ composite under visible light and the hybrid system with ultrafiltration, *Chem. Eng. J.*, 2020, **399**, 125733–125771.
 - 12 Q. F. Mei, F. Y. Zhang, N. Wang, Y. Yang, R. L. Wu and W. Wang, TiO₂/Fe₂O₃ heterostructures with enhanced photocatalytic reduction of Cr(VI) under visible light irradiation, *RSC Adv.*, 2019, **9**, 22764–22771.
 - 13 J. Wang, G. H. Wang, B. Cheng, J. G. Yu and J. J. Fan, Sulfur-doped g-C₃N₄/TiO₂ S-scheme heterojunction photocatalyst for Congo Red photodegradation, *Chin. J. Catal.*, 2021, **42**, 56–68.
 - 14 X. Li, Y. P. Deng, Z. M. Jiang, R. C. Shen, J. Xie, W. Liu and X. B. Chen, Photocatalytic Hydrogen Production over CdS Nanomaterials: An Interdisciplinary Experiment for Introducing Undergraduate Students to Photocatalysis and Analytical Chemistry, *J. Chem. Educ.*, 2019, **96**, 1224–1229.
 - 15 R. C. Shen, D. D. Ren, Y. N. Ding, Y. T. Guan, Y. H. Ng, P. Zhang and X. Li, Nanostructured CdS for efficient photocatalytic H₂ evolution: A review, *Sci. China Mater.*, 2020, **63**, 2153–2188.
 - 16 C. Lops, A. Ancona, K. D. Cesare, B. Dumontel, N. Garino, G. Canavese, S. Hernandez and V. Cauda, Sonophotocatalytic degradation mechanisms of Rhodamine B dye via radicals generation by micro- and nano-particles of ZnO, *Appl. Catal., B*, 2019, **243**, 629–640.
 - 17 R. D. Suryavanshi, S. V. Mohite, A. A. Bagade, S. K. Shaikh, J. B. Thorat and K. Y. Rajpure, Nanocrystalline immobilised ZnO photocatalyst for degradation of benzoic acid and methyl blue dye, *Mater. Res. Bull.*, 2018, **101**, 324–333.
 - 18 J. Wang, Z. Wang, B. Huang, Y. Ma, Y. Liu, X. Qin, X. Zhang and Y. Dai, Oxygen vacancy induced band-gap narrowing and enhanced visible light photocatalytic activity of ZnO, *ACS Appl. Mater. Interfaces*, 2012, **4**, 4024–4030.
 - 19 G. M. Neelgund and A. Oki, ZnO conjugated graphene: An efficient sunlight driven photocatalyst for degradation of organic dyes, *Mater. Res. Bull.*, 2020, **129**, 110911–110943.
 - 20 X. P. Qi, G. W. She, Y. Y. Liu, L. X. Mua and W. S. Shi, Electrochemical synthesis of CdS/ZnO nanotube arrays with excellent photoelectrochemical properties, *Chem. Commun.*, 2012, **48**, 242–244.
 - 21 X. Ma, F. Zhao, Q. Qiang, T. Liu and Y. Wang, Fabrication of selective interface of ZnO/CdS heterostructures for more efficient photocatalytic hydrogen evolution, *Dalton Trans.*, 2018, **47**, 12162–12171.
 - 22 G. Z. Huang, P. P. Zhang and Z. M. Bai, Self-powered UV-visible photodetectors based on ZnO/graphene/CdS/electrolyte heterojunctions, *J. Alloys Compd.*, 2019, **776**, 346–352.
 - 23 C. J. Zhang, N. J. Li, D. Y. Chen, Q. F. Xu, H. Li, J. H. He and J. M. Lu, The ultrasonic-induced-piezoelectric enhanced photocatalytic performance of ZnO/CdS nanofibers for degradation of bisphenol A, *J. Alloys Compd.*, 2021, **885**, 160987–160996.
 - 24 R. Afeesh, N. A.-M. Barakat, S. S. Al-Deyab, A. Yousef and H. Y. Kim, Nematic shaped cadmium sulfide doped electrospun nanofiber mat: Highly efficient, reusable, solar light photocatalyst, *Colloids Surf., A*, 2012, **409**, 21–29.
 - 25 H. Li, C. Z. Yao, L. X. Meng, H. Sun, J. Huang and Q. J. Gong, Photoelectrochemical performance of hydrogenated ZnO/CdS core-shell nanorod arrays, *Electrochim. Acta*, 2013, **108**, 45–50.
 - 26 Q. Yang, Y. Li, Z. Hu, Z. Duan, P. Liang, J. Sun, N. Xu and J. Wu, Extended photo-response of ZnO/CdS core/shell nanorods fabricated by hydrothermal reaction and pulsed laser deposition, *Opt. Express*, 2014, **22**, 8617–8623.
 - 27 A. Yousef, N. A.-M. Barakat, K. A. Khalil, A. R. Unnithan, G. Panthi, B. Pant and H. Y. Kim, Photocatalytic release of hydrogen from ammonia borane-complex using Ni(0)-doped TiO₂/C electrospun nanofibers, *Colloids Surf., A*, 2012, **410**, 59–65.
 - 28 P. W. Huo, M. J. Zhou, Y. F. Tang, X. L. Liu, C. C. Ma, L. B. Yu and Y. S. Yan, Incorporation of N-ZnO/CdS/Graphene oxide composite photocatalyst for enhanced photocatalytic activity under visible light, *J. Alloys Compd.*, 2016, **670**, 198–209.
 - 29 S. Juabrum, T. Chankhanittha and S. Nanan, Hydrothermally grown SDS-capped ZnO photocatalyst for degradation of RR141 azo dye, *Mater. Lett.*, 2019, **245**, 1–13.
 - 30 W. Xia, Y. Wang, Q. Wang, Y. Z. Yan and Y. J. Jiang, Tubular acceptor-rich ZnO hierarchical heterostructure as an efficient photocatalyst for organic degradation, *Appl. Surf. Sci.*, 2020, **506**, 145008–145016.
 - 31 J. Buasakun, P. Srilaoong, G. Chaloeipote, R. Rattanakram, C. Wongchoosuk and T. Duangthongyou, Synergistic effect of ZnO/ZIF8 heterostructure material in photodegradation of methylene blue and volatile organic compounds with sensor operating at room temperature, *J. Solid State Chem.*, 2020, **289**, 121494–121521.
 - 32 Y. T. Zhao, L. Li, Y. J. Zuo, G. Y. He, Q. Chen, Q. Meng and H. Q. Chen, Reduced graphene oxide supported ZnO/CdS



- heterojunction enhances photocatalytic removal efficiency of hexavalent chromium from aqueous solution, *Chemosphere*, 2021, **286**, 131738–131746.
- 33 T. Y. Peng, K. Li, P. Zeng, Q. G. Zhang and X. G. Zhang, Enhanced Photocatalytic Hydrogen Production over Graphene Oxide-Cadmium Sulfide Nanocomposite under Visible Light Irradiation, *J. Phy. Chem. C*, 2012, **116**, 22720–22726.
- 34 A. Y. Meng, B. C. Zhu, B. Zhong, L. Y. Zhang and B. Cheng, Direct Z-scheme TiO₂/CdS hierarchical photocatalyst for enhanced photocatalytic H₂-production activity, *Appl. Surf. Sci.*, 2017, **422**, 518–527.
- 35 X. Y. Li, D. Wu, Q. Z. Luo, J. An, R. Yin and D. S. Wang, Advanced cyclized polyacrylonitrile (CPAN)/CdS nanocomposites for highly efficient visible-light photocatalysis, *J. Mater. Sci.*, 2016, **52**, 736–748.
- 36 Y. Li, X. Li, H. W. Zhang, J. J. Fan and Q. J. Xiang, Design and application of active sites in g-C₃N₄-based photocatalysts, *J. Mater. Sci. Technol.*, 2020, **56**, 69–88.
- 37 H. Cheng, J. Y. Wang, Y. Z. Zhao and X. J. Han, Effect of phase composition, morphology, and specific surface area on the photocatalytic activity of TiO₂ nanomaterials, *RSC Adv.*, 2014, **4**, 47031–47038.
- 38 J. X. Bai, R. C. Shen, W. L. Chen, J. Xie, P. Zhang, Z. M. Jiang and X. Li, Enhanced photocatalytic H₂ evolution based on a Ti₃C₂/Zn_{0.7}Cd_{0.3}S/Fe₂O₃ Ohmic/S-scheme hybrid heterojunction with cascade 2D coupling interfaces, *Chem. Eng. J.*, 2022, **429**, 132587–132599.
- 39 R. C. Shen, Y. N. Ding, S. B. Li, P. Zhang, Q. J. Xiang, Y. H. Ng and X. Li, Constructing low-cost Ni₃C/twin-crystal Zn_{0.5}Cd_{0.5}S heterojunction/homojunction nanohybrids for efficient photocatalytic H₂ evolution, *Chin. J. Catal.*, 2021, **42**, 25–36.
- 40 D. D. Ren, W. A. Zhang, Y. N. Ding, R. C. Shen, Z. M. Jiang, X. Y. Lu and X. Li, In-situ fabricating robust cocatalyst-free CdS/g-C₃N₄ 2D-2D step-scheme heterojunctions for highly active H₂ evolution, *Sol. RRL*, 2019, **4**, 1900423–1900432.
- 41 K. M. Cho, K. H. Kim, K. Park, C. Kim, S. Kim, A. Al-Saggaf, I. Gereige and H. Jung, Amine-Functionalized Graphene/CdS Composite for Photocatalytic Reduction of CO₂, *ACS Catal.*, 2017, **7**, 7064–7069.
- 42 M. B. Menon, A. M. Raj and G. T. Chirayil, Tunable direct band gap photoluminescent organic semiconducting nanoparticles from lignite, *Sci. Rep.*, 2017, **7**, 18012–18020.
- 43 L. Kaliraj, J. C. Ahn, E. J. Rupa, S. Abid, J. Lu and D. C. Yang, Synthesis of panos extract mediated ZnO nano-flowers as photocatalyst for industrial dye degradation by UV illumination, *J. Photochem. Photobiol., B*, 2019, **199**, 111588–111611.
- 44 X. J. Zhai, Y. J. Xia, D. J. Sun and J. Xu, Cd²⁺ Counterion-Assisted Synthesis of Uniform CdS Nanospheres Capped with the Anionic Surfactant Sodium dodecylsulfate, *J. Dispersion Sci. Technol.*, 2013, **35**, 76–83.
- 45 S. S. Warule, N. S. Chaudhari, B. B. Kale and M. A. More, Novel sonochemical assisted hydrothermal approach towards the controllable synthesis of ZnO nanorods, nanocups and nanoneedles and their photocatalytic study, *CrystEngComm*, 2009, **11**, 2776–2783.
- 46 Z. D. Wei, M. Q. Xu, J. Y. Liu, W. Q. Guo, Z. Jiang and W. F. Shangguan, Simultaneous visible-light-induced hydrogen production enhancement and antibiotic wastewater degradation using MoS₂@Zn Cd1-S: Solid-solution-assisted photocatalysis, *Chin. J. Catal.*, 2020, **41**, 103–113.
- 47 Y. G. Lei, X. W. Wu, S. H. Li, J. Y. Huang, K. H. Ng and Y. K. Lai, Noble-metal-free metallic MoC combined with CdS for enhanced visible-light-driven photocatalytic hydrogen evolution, *J. Cleaner Prod.*, 2021, **322**, 129018–129062.
- 48 S. Singh and N. Khare, CdS/ZnO core/shell nano-heterostructure coupled with reduced graphene oxide towards enhanced photocatalytic activity and photostability, *Chem. Phys. Lett.*, 2015, **634**, 140–145.
- 49 Q. Q. Yu, J. Y. Chen, Y. X. Li, M. C. Wen, H. L. Liu, G. Y. Li and T. C. An, In-situ decoration of metallic Bi on BiOBr with exposed (110) facets and surface oxygen vacancy for enhanced solar light photocatalytic degradation of gaseous n-hexane, *Chin. J. Catal.*, 2020, **41**, 1603–1612.
- 50 R. C. Shen, X. Y. Lu, Q. Q. Zheng, Q. Chen, Y. H. Ng, P. Zhang and X. Li, Tracking S-Scheme Charge Transfer Pathways in Mo₂C/CdS H₂-Evolution Photocatalysts, *Sol. RRL*, 2021, **5**, 2100177–2100183.
- 51 Z. Z. Liang, R. C. Shen, Y. H. Ng, P. Zhang, Q. J. Xiang and X. Li, A review on 2D MoS₂ cocatalysts in photocatalytic H₂ production, *J. Mater. Sci. Technol.*, 2020, **56**, 89–121.
- 52 Z. M. Jiang, Q. Chen, Q. Q. Zheng, R. C. Shen, P. Zhang and X. Li, Constructing 1D/2D Schottky-based heterojunctions between Mn_{0.2}Cd_{0.8}S nanorods and Ti₃C₂ nanosheets for boosted photocatalytic H₂ evolution, *Acta Phys.-Chim. Sin.*, 2021, **37**, 2010059.
- 53 R. A. He, R. Chen, J. H. Luo, S. Y. Zhang and D. F. Xu, Fabrication of graphene quantum dots modified BiOI/PAN flexible fiber with enhanced photocatalytic activity, *Acta Phys.-Chim. Sin.*, 2020, **37**, 2011022.
- 54 X. J. Wen, L. Qian, X. X. Lv, J. Sun, J. Guo, Z. H. Fei and C. G. Niu, Photocatalytic degradation of sulfamethazine using a direct Z-Scheme AgI/Bi₄V₂O₁₁ photocatalyst: Mineralization activity, degradation pathways and promoted charge separation mechanism, *J. Hazard. Mater.*, 2020, **385**, 121508–121548.
- 55 G. Z. Wang, L. Geng, W. Y. Tang, B. Wang, W. X. Zhao, W. L. Zhang, B. F. Yuan, H. K. Yuan and T. W. Zhou, Two dimensional CdS/ZnO type-II heterostructure used for photocatalytic water-splitting, *Nanotechnology*, 2020, **31**, 485701.
- 56 X. Q. Qiao, Z. W. Zhang, Q. H. Li, D. F. Hou, Q. C. Zhang, J. Zhang, D. S. Li, P. Y. Feng and X. H. Bu, In situ synthesis of n-n Bi₂MoO₆ & Bi₂S₃ heterojunctions for highly efficient photocatalytic removal of Cr(VI), *J. Mater. Chem. A*, 2018, **6**, 22580–22589.
- 57 J. Aliaga, N. Cifuentes, G. González, C. Sotomayor-Torres and E. Benavente, Enhancement Photocatalytic Activity of the Heterojunction of Two-Dimensional Hybrid Semiconductors ZnO/V₂O₅, *Catalysts*, 2018, **8**, 374–386.
- 58 S. Y. Janbandhu, A. Joshi, S. R. Munishwar and R. S. Gedam, CdS/TiO₂ heterojunction in glass matrix: Synthesis, characterization, and application as an improved photocatalyst, *Appl. Surf. Sci.*, 2019, **497**, 143758–143804.



- 59 T. Senasu, T. Chankhanittha, K. Hemavibool and S. Nanan, Visible-light-responsive photocatalyst based on ZnO/CdS nanocomposite for photodegradation of reactive red azo dye and ofloxacin antibiotic, *Mater. Sci. Semicond. Process.*, 2021, **123**, 105558–105571.
- 60 F. Z. Liu, Y. H. Leung, A. B. Djurišić, A. M.-C. Ng and W. K. Chan, Native Defects in ZnO: Effect on Dye Adsorption and Photocatalytic Degradation, *J. Phys. Chem. C*, 2013, **117**, 12218–12228.
- 61 M. X. Chen, C. Z. Bao, T. X. Cun and Q. Huang, One-pot synthesis of ZnO/oligoaniline nanocomposites with improved removal of organic dyes in water: Effect of adsorption on photocatalytic degradation, *Mater. Res. Bull.*, 2017, **95**, 459–467.
- 62 Z. L. Guan, X. M. Li, Y. Wu, Z. Chen, X. D. Huang, D. B. Wang, Q. Yang, J. L. Liu, S. H. Tian, X. Y. Chen and H. Zhao, AgBr nanoparticles decorated 2D/2D GO/Bi₂WO₆ photocatalyst with enhanced photocatalytic performance for the removal of tetracycline hydrochloride, *Chem. Eng. J.*, 2021, **410**, 128283–128295.
- 63 S. Q. Wu, H. Y. Hu, Y. Lin, J. L. Zhang and Y. H. Hu, Visible light photocatalytic degradation of tetracycline over TiO₂, *Chem. Eng. J.*, 2020, **382**, 122842–122851.
- 64 D. Ramimoghadam, M. Z. Hussein and Y. H. Taufiq-Yap, The effect of sodium dodecyl sulfate (SDS) and cetyltrimethylammonium bromide (CTAB) on the Properties of ZnO synthesized by hydrothermal method, *Int. J. Mol. Sci.*, 2012, **13**, 13275–13293.
- 65 B. Neppolian, H. C. Choi, S. Sakthivel, B. Arabindoo and V. Murugesan, Solar light induced and TiO₂ assisted degradation of textile dye reactive blue 4, *Chemosphere*, 2002, **46**, 1173–1181.
- 66 W. Z. Tang and H. An, Photocatalytic degradation kinetics and mechanism of acid blue 40 by TiO₂/UV in aqueous solution, *Chemosphere*, 1995, **31**, 4171–4183.
- 67 Y. B. Zhao, Y. X. Ci and W. B. Chang, Fluorescence enhancing by alkaline degradation of tetracycline antibiotics and its application, *Sci. China, Ser. B: Chem.*, 1997, **40**, 434–441.
- 68 D. Das and P. Nandi, Ternary ZnCdSO composite photocatalyst for efficient dye degradation under visible light retaining Z-scheme of migration pathways for the photo-generated charge carriers, *Sol. Energy Mater. Sol. Cells*, 2020, **217**, 110674–110685.
- 69 S. J. Li, C. C. Wang, M. J. Cai, F. Yang, Y. P. Liu, J. L. Chen, P. Zhang, X. Li and X. B. Chen, Facile fabrication of TaON/Bi₂MoO₆ core-shell S-scheme heterojunction nanofibers for boosting visible-light catalytic levofloxacin degradation and Cr(VI) reduction, *Chem. Eng. J.*, 2022, **428**, 131158–131172.
- 70 F. Du, Z. Lai, H. Tang, H. Wang and C. Zhao, Construction and application of BiOCl/Cu-doped Bi₂S₃ composites for highly efficient photocatalytic degradation of ciprofloxacin, *Chemosphere*, 2022, **287**, 132391–132401.
- 71 Y. L. Jia, Z. Z. Wang, X. Q. Qiao, L. Huang, S. L. Gan, D. F. Hou, J. Zhao, C. H. Sun and D. S. Li, A synergistic effect between S-scheme heterojunction and Noble-metal free cocatalyst to promote the hydrogen evolution of ZnO/CdS/MoS₂ photocatalyst, *Chem. Eng. J.*, 2021, **424**, 130368–130382.
- 72 K. Divakaran, A. Baishnisha, V. Balakumar, K. N. Perumal, C. Meenakshi and R. S. Kannan, Photocatalytic degradation of tetracycline under visible light using TiO₂@sulfur doped carbon nitride nanocomposite synthesized via in-situ method, *J. Environ. Chem. Eng.*, 2021, **9**, 105560–105570.
- 73 D. Ma, J. W. Shi, Y. Zou, Z. Fan, X. Ji and C. Niu, Highly Efficient Photocatalyst Based on a CdS Quantum Dots/ZnO Nanosheets 0D/2D Heterojunction for Hydrogen Evolution from Water Splitting, *ACS Appl. Mater. Interfaces*, 2017, **9**, 25377–25386.
- 74 Q. Z. Du, P. Wu, Y. Y. Sun, J. Y. Zhang and H. He, Selective photodegradation of tetracycline by molecularly imprinted ZnO@NH₂-UiO-66 composites, *Chem. Eng. J.*, 2020, **390**, 124614–124624.
- 75 E. H. Jiang, X. T. Liu, H. N. Che, C. B. Liu, H. J. Dong and G. B. Che, Visible-light-driven Ag/Bi₃O₄Cl nanocomposite photocatalyst with enhanced photocatalytic activity for degradation of tetracycline, *RSC Adv.*, 2018, **8**, 37200–37207.
- 76 C. T. Hou, H. Y. Liu and Y. J. Li, The preparation of three-dimensional flower-like TiO₂/TiOF₂ photocatalyst and its efficient degradation of tetracycline hydrochloride, *RSC Adv.*, 2021, **11**, 14957–14969.
- 77 F. Su, P. P. Li, J. S. Huang, M. J. Gu, Z. Y. Liu and Y. H. Xu, Photocatalytic degradation of organic dye and tetracycline by ternary Ag₂O/AgBr-CeO₂ photocatalyst under visible-light irradiation, *Sci. Rep.*, 2021, **11**, 85–97.
- 78 Y. Wang, D. D. Wang, H. J. Li, W. Jiang, C. B. Liu and G. B. Che, A visible-light-driven 3D Z-scheme photocatalyst by loading BiOI nanosheets onto g-C₃N₄ microtubes for efficient degradation of tetracycline and p-chlorophenol, *J. Mater. Sci.*, 2021, **56**, 5555–5569.
- 79 W. J. Zhang, Y. X. Ma, X. H. Zhu, S. J. Liu, T. An, J. Y. Bao, X. Y. Hub and H. W. Tian, Fabrication of Ag decorated g-C₃N₄/LaFeO₃ Z-scheme heterojunction as highly efficient visible-light photocatalyst for degradation of methylene blue and tetracycline hydrochloride, *J. Alloys Compd.*, 2021, **864**, 158914–158925.
- 80 A. M. Al-Enizi, M. M. El-Halwany, M. A. Al-Abdrabnabi, M. Bakrey, M. Ubaidullah and A. Yousef, Novel Low Temperature Route to Produce CdS/ZnO Composite Nanofibers as Effective Photocatalysts, *Catalysts*, 2020, **10**, 417–427.
- 81 R. C. Pawar and C. S. Lee, Single-step sensitization of reduced graphene oxide sheets and CdS nanoparticles on ZnO nanorods as visible-light photocatalysts, *Appl. Catal., B*, 2014, **144**, 57–65.
- 82 M. Khan, M. H. Irfan, M. Israr, N. Rehman, T. J. Park and M. A. Basit, Comparative investigation of ZnO morphologies for optimal CdS quantum-dot deposition via pseudo-SILAR method, *Chem. Phys. Lett.*, 2020, **744**, 137223–137241.
- 83 C. Venkatarreddy, N. Bandaru, I. N. Reddy, J. Shim and K. Yoo, UV-visible light driven photocatalytic activities of CdS nanoparticles supported ZnO layers, *Mater. Sci. Eng., B*, 2018, **232–235**, 68–75.

